Journal of Ceramic Processing Research. Vol. 14, No. 3, pp. 396~399 (2013)

J O U R N A L O F
Ceramic Processing Research

Effect of Al concentration on the structural and optical properties of Al-doped ZnO nanorods grown on indium-tin-oxide-coated glass substrates by using a templateless electrochemical deposition method

Young Soo No and Tae Whan Kim[1,*]

Department of Electronics and Computer Engineering, Hanyang University, 17 Haengdang-dong, Seongdong-gu, Seoul 133-791, Korea

Al-doped ZnO (AZO) nanorods were formed on indium-tin-oxide (ITO)-coated glass substrates by using a templateless electrochemical deposition method. X-ray photoelectron spectroscopy spectra showed that the stoichiometry of the samples were Al 2p, Zn 2p, and O 1s peaks, indicative of the formation of AZO nanorods. Scanning electron microscopy images showed that the density of the AZO nanorods decreased with increasing Al concentration. X-ray diffraction patterns showed that the d-spacing of the (002) plane for the AZO nanorods decreased with increasing Al concentration. Photoluminescence spectra for the AZO nanorods formed on the ITO-coated glass substrates showed that the dominant emission peak related to the band-to-band transitions shifted to a higher wavelength side with increasing Al concentration.

PACS: **78.55.Et, 78.66.Sq, 78.67.Bf**
Key words: Al-doped ZnO nanorod, Structural property, Optical property, Electrochemical deposition method.

Introduction

ZnO thin films have currently emerged as excellent candidates for potential applications in electronic and optoelectronic devices, such as light-emitting diodes [1], ultraviolet laser diodes [2], solar cells [3], photodetectors [4], and thin film transistors [5] because they are large band-gap semiconductors with novel physical properties of large exciton binding energies and excellent chemical stabilities [6, 7]. The prospect of potential applications of optoelectronic devices utilizing ZnO thin films has led to substantial research and development efforts to form various types of nanostructures, acting as functioning regions [8-10]. Synthesis methods, such as physical vapor deposition [8], chemical vapor deposition [10], and pulsed laser deposition [9] have been extensively used to achieve high-quality ZnO nanostructures. Among the various synthesis methods, an electrochemical deposition (ECD) method has been used to form ZnO nanostructures due to its advantages of a high growth rate, fabrication over a large area, and low cost [11-13]. Among the various kinds of doped ZnO nanostructures, Al-doped ZnO (AZO) nanorods have emerged as excellent candidates for the fabrication of transparent conducting electrodes because they are more stable in a reducing ambient, more abundant, and less expensive than indium-tin-oxide films [14-18]. While the high optical transparency of the AZO nanorods in the visible spectral range is maintained, their conductivity significantly decreases in comparison with that of the ZnO thin films, resulting in the utilization of the electrodes. Even though some investigations on the formation and physical properties of AZO nanostructures have been carried out, studies concerning the effect of Al concentration on the structural and optical properties of the AZO nanorods have not been performed yet. Furthermore, systematic studies concerning the effect of Al concentration on the structural and optical properties of AZO nanorods are necessary to enhance device efficiency.

This paper reports the effect of Al concentration on the structural and optical properties of ZnO nanorods formed on indium-tin-oxide (ITO) coated glass substrates by the ECD method. X-ray photoelectron spectroscopy (XPS) measurements were performed to investigate the stoichiometry of the samples. Scanning electron microscopy (SEM) and X-ray diffraction (XRD) measurements were performed to characterize the structural properties of the formed ZnO nanorods. Photoluminescence (PL) measurements were performed to investigate the optical properties of the ZnO nanorods.

Experimental Details

The AZO nanorods used in this work were formed on ITO-coated glass substrates by ECD. The resistivity of the ITO film was 17 Ω/square. The AZO nanorods were formed by the reduction of dissolved molecular oxygen in zinc nitrate hexahydrate and various amount

*Corresponding author:
Tel : +82-2-2220-0354
Fax: +82-2-2292-4135
E-mail: twk@hanyang.ac.kr

of $Al(NO_3)_3 9H_2O$ solution [19, 20]. The electrochemical reduction of oxygen molecules generates AZO nanorods from the combination between the precursor and the current of the cathode [21, 22]. The shape and crystal structure of the AZO nanostructures were controlled by varying the growth conditions of ECD. The ECD equipment used for the growth of AZO nanostructures consisted of three electrode electrochemical cells with an ITO cathode, acting as a working electrode. While an Ag/AgCl (3 M NaCl) electrode was used as a reference electrode, the platinum served as a counter electrode. $Zn(NO_3)_2 \cdot 6H_2O$ (1 mM) and KCl were dissolved in 250 ml of deionized water. The KCl (Sigma-Aldrich, 99.0-100.5%) acted as a supporting precursor [22], and the $Zn(NO_3)_2 \cdot 6H_2O$ (Sigma-Aldrich, 98.0%) acted as a Zn^{2+} precursor. AZO nanorods were formed by using Al concentrations of 0, 2, or 3.3 wt%. The ZnO nanorods were electrochemically deposited at 75 °C under a constant applied voltage of -1.1 V for 10 min.

XPS measurements were performed using a VG Multilab ESCA 2000 system with a monochromated Mg Kα X-ray source (1253.6 eV) at a constant analyzer pass energy of 40 eV. All obtained spectra were calibrated to a C 1s electron peak at 284.5 eV. XPS investigations of the electronic states of the samples were conducted in a VG Multilab ESCA 2000 system using a monochromated Mg Kα X-ray source (1253.6 eV). Field-emission SEM measurements were performed using a JSM-6330F scanning electron micro-scope. XRD measurements were carried out using a Rigaku D/MAX-2500 diffractometer with Cu Kα radiation, which was operated at a scanning speed of 5 °/min for a 2θ range between 20 ° and 70 °. The X-ray tube voltage and current were set at 40 kV and 100 mA, respectively. PL measurements were carried out using a 50 cm monochromator equipped with an RCA 31034 photomultiplier tube. The excitation source was the 325 nm line of a He-Cd laser, and the sample temperature was kept at 300 K.

Results and Discussion

Figure 1 shows XPS spectra of AZO nanorods formed by using Al concentrations of 0, 2, or 3.3 wt%. XPS spectra for the samples grown at Al concentrations of 0, 2, or 3.3 wt% depict Al 2p and O 1s core levels, as shown in Fig. 1(a) and 1(b). The position of the dominant Al 2p peak at 73.94 eV is smaller than that at 74.4 eV corresponding to the Al 2p peak in the Al_2O_3 material. Al^{2+} atoms are substitutively incoporated into the ZnO lattice because the binding energy can be changed due to the energy transfer between the matrix ions and the dopants. The O 1s peak at 529.6 eV for the XPS spectra shown in Fig. 1(b) is attributed to oxide ions in the ZnO crystal lattice. The peak around 531.6 eV for the Fig. 1(b) is related to the Zn-O binding energy, indicative of the oxygen deficient state for the AZO nanorods. The OH or water covered ZnO

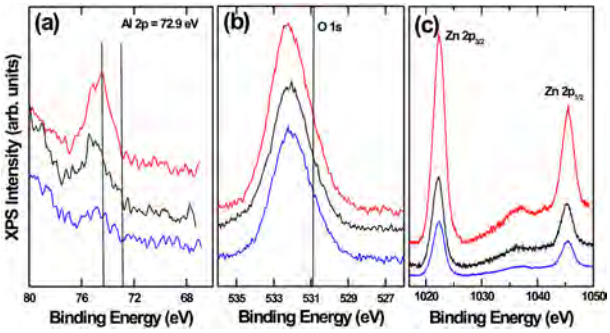

Fig. 1. X-ray photoemission spectroscopy narrow scan spectra for (a) Al 2p, (b) O 1s, and (c) Zn 2p peaks for the Al-doped ZnO nanorods deposited on ITO substrates with Al concentrations of 0, 2, and 3.3 wt%.

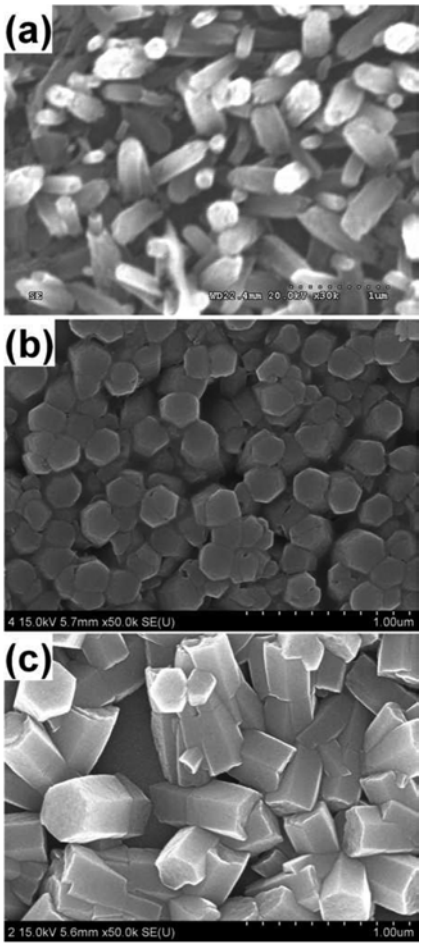

Fig. 2. Scanning electron microscopy images of the Al-doped ZnO nanorods deposited on ITO substrates with Al concentrations of (a) 0, (b) 2, and (c) 3.3 wt%.

nanorods might become negligible with increasing Al dopant. The Zn 2p core-level photoemission (PE) spectra of the ZnO nanorods are shown in Fig. 1(c). The shoulder around 1021.4 eV indicates that the oxidation state of the Zn $2p_{3/2}$ is similar to that of the ZnO bulk. The peak position and the intensity of the Zn 2p peak are not significantly affected by Al concentration. The strong intensity of the Zn $2p_{3/2}$ ($2p_{1/2}$)

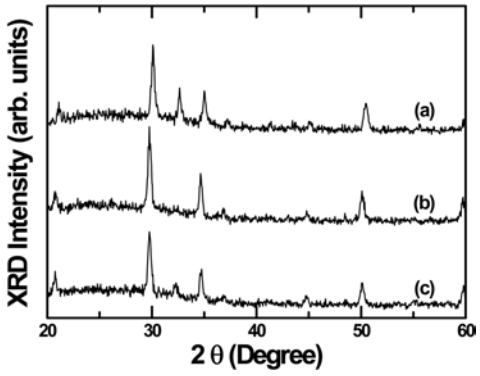

Fig. 3. X-ray diffraction curves of the Al-doped ZnO nanorods deposited on the indium-tin-oxide-coated glass substrates with Al concentrations of (a) 0, (b) 2, and (c) 3.3 wt%.

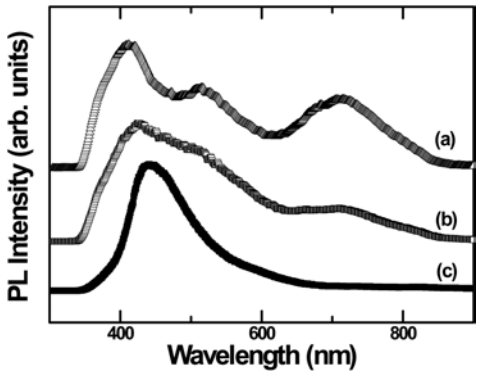

Fig. 4. Photoluminescence spectra for the Al-doped ZnO nanorods at room temperature with Al concentrations of (a) 0, (b) 2, and (c) 3.3 wt%.

peak indicates that a single Zn^{2+} divalent state corresponds to both the $Zn(OH)_2$ and the ZnO. The spin-orbit splitting energy of 22.9 eV for the Zn $2p_{3/2}$ ($2p_{1/2}$) is in reasonable agreement with that reported in the literature [23]. The SEM images of AZO nanorods grown with differnet Al concentrations of (a) 0, (b) 2, and (c) 3.3 wt% are shown in Fig. 3. The diameter of the AZO nanorods increases with increasing Al concentration due to an increase in the size of the AZO nanorods.

Figure 3 shows the XRD patterns of the AZO nanorods formed by using different Al concentraions of (a) 0, (b) 2, and (c) 3 wt%. The XRD patterns show that the AZO nanorods have polycrystalline hexagonal wurzite structures with lattice parameters of a = 3.249 and c = 5.206 Å, which are in resonable agreement with the literature values (JCPDS card, No. 36-1451). No phase corresponding to Al related compounds is obsereved in the XRD patterns. The Al doping on the ZnO nanorods shifts the (002) peak position toward a larger 2θ value in comparison with the peak for the undoped ZnO nanorods. The larger side shift of the peak for the AZO nanorods is attributed to the decrease of the lattice spacing between the (002) planes resulting from the substitution of Al^{3+} into Zn^{2+} sites. The XRD results depicts that the d-spacing of the (002) plane for the nanorods decreases from 2.585 to 2.560 Å with increasing Al concentration from 0 to 3.3 wt%, which is in reasonable agreement with the results reported in the literlature [24].

Figure 4 shows the PL spectra at 300 K for the ZnO nanorods formed by using different Al concentrations from 0 to 3.3 wt%. The full width at half maximum (FWHM) of the UV emissions for the PL spectra is approximately between 0.13 and 0.14 eV, which is smaller than that of ZnO bulk powder (0.22 eV) [25]. All the AZO nanorods exhibit UV emissions and broad visible emissions in the range between 470 and 630 nm. The PL spectrum of the undoped ZnO nanorods shown in Fig. 4 posses a borad emission peak in a UV region corresponding to the ZnO band gap. The position of the UV emission peak slightly shifts a larger wavelength side with increasing Al concentration. The redshift of the UV emission peak in the AZO nanorods originates from the sp-d hybridization or exchange interation between localized 3d electrons of the substitutional ions and conduction band eletrons. The increase in the UV peak inensity is related to the formation of the impurity defects resulting from an increase in the Al concentration.

Summary and Conclusion

The effect of the Al concentration on the structural and optical properties of the AZO nanorods formed on ITO-coated glass substrates by ECD was investigated. XPS spectra of the grown samples contained Al 2p, Zn 2p, and O 1s peaks, indicative of the formation of AZO nanorods. SEM images showed that the size of the AZO nanorods increased with increasing Al concentration. XRD patterns showed that the d-spacing of the (002) plane for the AZO nanorods decreased with increasing Al concentration. PL spectra at 300 K for the AZO nanorods showed that the dominant emission peak related to the band-to-band transitions shifted to a higher wavelength side with increasing Al concentration. An orange-red band corresponding to the oxygen-rich states and a blue emission band related to the oxygen vacancies appeared in the PL spectra. These results can help improve understanding of the effect of Al concentration on the structural and optical properties of AZO nanorods.

Acknowledgments

This research was supported by Basic Science Research Program through the National Research Foundation of Korea (NRF) funded by the Ministry of Education, Science and Technology (2013-016467).

References

1. J.H. Choi, H. Tabata, and T. Kawai, J. Cryst. Growth 226

(2001) 493-500.
2. J.H. Schön, A. Dodabalapur, Ch. Kloc, and B. Batlogg, Science 290 (2000) 963-965.
3. T. Soki, Y. Hatanaka, and D.C. Look, Appl. Phys. Lett. 76 (2000) 3257-3258.
4. A. Tsukazak, A. Ohtomo, T. Onuma, M. Ohtani, T. Makino, M. Sumiya, K. Ohtani, S.F. Chichibu, S. Fuke, Y. Segawa, H. Ohno, H. Koinuma, and M. Kawasaki, Nat. Mater. 4 (2005) 42-46.
5. H. Tsubomura, M. Matsumura, Y. Nomura, and T. Amamiya, Nature 261 (1976) 402-403.
6. Y. Chen, D.M. Bagnall, H.J. Ko, K.T. Park, K. Hiraga, Z. Zhu, and T. Tao, J. Appl. Phys. 84 (1998) 3912-3918.
7. S. Hong, H. Ko, Y. Chen, and T. Yao, J. Cryst. Growth 209 (2000) 537-541.
8. W.I. Park, D.H. Kim, S.W. Jung, and G.C. Yi, Appl. Phys. Lett. 80 (2002) 4232-4234.
9. J. Zuniga-Perez, A. Rahm, C. Czekalla, J. Lenzner, M. Lorenz, and M. Grundmann: Nanotechnology 18 (2007) 195303-195307.
10. D. Pradhan and K. T. Leung, Langmuir 24 (2008) 9707-9716.
11. R. Tena-Zaera, J. Elias, C. Lévy-Clément, C. Bekeny, T. Voss, I. Mora-Seró, and J. Bisquert: J. Phys. Chem. C 112 (2008) 16318-16323.
12. Y. Mastai, D. Gal, and G. Hodes, J. Electrochem. Soc. 147 (2000) 1435-.1439
13. H.Y. Yang, S.H. Lee, and T.W. Kim, Appl. Surf. Sci. 256 (2010) 6117-6120.
14. M. Grätzel, Nature 414 (2001) 338-344.
15. K. Nomura, H. Ohta, K. Ueda, T. Kamiya, M. Hirano, and H. Hosono, Science 300 (2003) 1269-1272.
16. R.F. Carcia, R.S. McLean, M.H. Reilly, and G. Nunes, Jr., Appl. Phys. Lett. 82 (2003) 1117-1119.
17. B.E. Sernelius, K-F. Berggren, Z-C. Jin, I. Hamberg, and C. G. Granqvist, Phys. Rev. B 37 (1988) 10244-10248.
18. J.M. Yuk, J.Y. Lee, J.H. Jung, D.U. Lee, T.W. Kim, D.I. Son, and W.K. Choi, Appl. Phys. Lett. 93 (2008) 221910-221913.
19. S. Peulon and D. Lincot, Adv. Mater. 8 (1996) 166-170.
20. R. Könenkamp, K. Boedecker, M.C. Lux-Steiner, M. Poschenrieder, F. Zenia, C. Lévy-Clément, and S. Wagner, Appl. Phys. Lett. 77 (2000) 2575-2578.
21. S. Štrbac and R.R. Adžiæ, Electrochim. Acta 41 (1996) 2903-2908.
22. S.P. Jiang, C.Q. Cui, and A.C.C. Tseung, J. Electrochem. Soc. 138 (1991) 3599-3605.
23. J.F. Moulder, W.F. Stickle, P.E. Sobol, and K.D. Bomben: *Handbook of X-ray Photoelectron Spectroscopy*, ed. J. Chastain (Perkin-Elmer, Eden Prairie, MN, 1992).
24. C.S. Prajapati and P.P. Sahay, Cryst. Res. Technol. 46 (2011) 1086-1092.
25. C. Geng, Y. Jiang, Y. Yao, X. Meng, J.A. Zapien, C.S. Lee, Y. Lifshitz, and S.T. Lee: Adv. Funct. Mater. 14 (2004) 589-594.